Frontiers of Information Technology & Electronic Engineering
www.jzus.zju.edu.cn; engineering.cae.cn; www.springerlink.com
ISSN 2095-9184 (print); ISSN 2095-9230 (online)
E-mail: jzus@zju.edu.cn

Correspondence:

Three-dimensional-printed low-sidelobe dual-band dual-polarized antenna array for Ku-band satellite communications*

Yuqi XIA[1,2,3,4], Xiuping LI[1,2,3,4], Genqiang KOU[1,2,3,4], Wenyu ZHAO[1,2,3,4], Jie ZHANG[1,2,3,4], Muhammad ISHFAQ[1,2,3,4], Zihang QI†‡[1,2,3,4]

[1]*State Key Laboratory of Information Photonics and Optical Communications, Beijing 100876, China*

[2]*Key Laboratory of Universal Wireless Communications of Ministry of Education, Beijing 100876, China*

[3]*Beijing Key Laboratory of Work Safety Intelligent Monitoring, Beijing 100876, China*

[4]*School of Electronic Engineering, Beijing University of Posts and Telecommunications, Beijing 100876, China*

†E-mail: qizihang@bupt.edu.cn

Received Aug. 13, 2024; Revision accepted Dec. 22, 2024; Crosschecked July 18, 2025

https://doi.org/10.1631/FITEE.2400709

A 3D-printed dual-band dual-polarization gap waveguide (GWG) slot antenna array is presented for Ku-band satellite communications (SATCOMs) in this paper. Two stacked GWGs excite the quasi-TE_{420} and quasi-TE_{240} modes in the cavity separately through orthogonal slots. An unequal power divider with a large power division ratio is proposed based on a ridge gap waveguide (RGW). Two power tapering distribution networks are realized for dual polarizations, and the sidelobe level (SLL) is suppressed. The antenna is fabricated in parts by direct metal laser sintering (DMLS), and the whole antenna is obtained by screw assembly. The measured impedance bandwidth well covers both the transmitting band (Tx, from 14.0 GHz to 14.5 GHz) and the receiving band (Rx, from 12.25 GHz to 12.75 GHz) required for Ku-band SATCOMs. Measurement results show that the maximum gain reaches 25.6 dBi, and that the radiation efficiency of the dual-band is >72%.

1 Introduction

Satellite communications (SATCOMs) have the advantages of wide coverage, long communication distance, and little impact of natural disasters. As a commonly used frequency band for SATCOM, the Ku band covers 13.7–14.5 GHz and 10.70–12.75 GHz, which are used for uplink and downlink data transmission, respectively (Zhang JJ et al., 2022). At the same time, to reduce the number of antennas in transceiver systems, dual-polarized antennas are usually adopted (Zhao et al., 2017; Yu et al., 2023). Considering that a high-throughput satellite system often requires high effective isotropic radiated power (EIRP) (Fenech et al., 2015), antennas are required to have high power capacity and high gain performance (Dimitrov et al., 2020; Garcia-Marin et al., 2021). Therefore, waveguide dual-polarized antenna becomes another feasible scheme (Chen et al., 2020; Cheng et al., 2020; You et al., 2022; Zhang J et al., 2022; Lu et al., 2023). However, waveguide antennas require cooperated feeding networks, which makes the antenna very complex and large (Sun et al., 2022), so high processing accuracy is required (Miura et al., 2011). Gap waveguide (GWG) has similar

‡ Corresponding author

* Project supported by the National Natural Science Foundation of China (Nos. 62321001 and 62301065)

ORCID: Zihang QI, https://orcid.org/0000-0002-5488-6404

transmission characteristics to waveguides and has lower requirements for processing. A large number of studies have proved that it is suitable for designing high-gain antennas (Zaman and Kildal, 2014; Akbari et al., 2019; Ferrando-Rocher et al., 2019a, 2019b). In Ferrando-Rocher et al. (2019b), the Ka-band 8×8 dual-polarized antenna showed a high gain of 27 dBi. However, the physical sizes of the antennas are large, resulting in high sidelobe levels (SLLs). A common way to reduce SLL is to introduce an amplitude-tapering feeding network (Jiang et al., 2019; Ran et al., 2022). A method suitable for GWG to design an unequal T-junction was proposed by Ran et al. (2022). Unfortunately, the antenna requires an additional layer of power divider to compensate for the phase inversion of adjacent units caused by the feeding method, thus sacrificing some gain.

In this paper, a dual-band dual-polarized antenna with both high gain and low SLL is proposed. The high-gain design is guided by mode analysis in the cavity. To realize the two-dimensional (2D) tapered amplitude distribution, an unequal T-junction power divider with a large power division ratio is proposed. Limited by the physical size of the unit feed structure, the power distributor adopts the combined groove ridge gap waveguide (RGW) to achieve a compact feeding network. Based on the structural characteristics of GWG, the antenna is processed by metal 3D printing techniques. The antenna is split into four layers for independent printing and finally obtained as a whole through screw assembly.

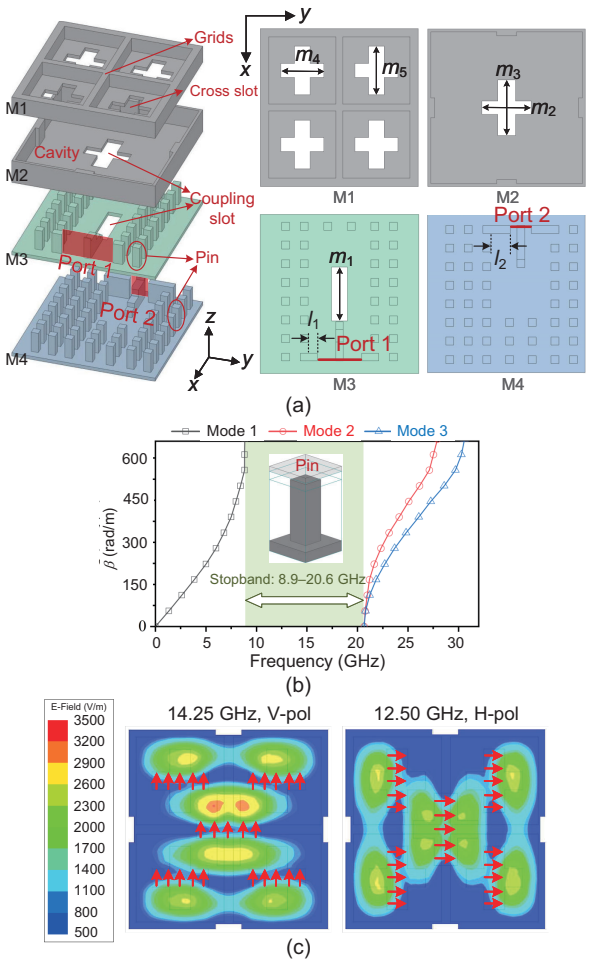

Fig. 1 Three-dimensional view and top view of the subarray (a), dispersion diagram of the pin (b), and electric field of the cavity (c)

2 Design of the subarray

The subarray consisting of a radiator and two feed GWGs is illustrated in Fig. 1a. GWGs use multiple rows of metal pins to prevent electromagnetic leakage. From the dispersion curve shown in Fig. 1b, it can be seen that its operating bandwidth ranges from 8.9 GHz to 20.6 GHz.

M1 and M2 together serve as the radiator of the subarray, which contains a 2×2 cross slot and a cavity. When the feeding ports are excited, the microwave is coupled from the feed layer to the cavity and radiated out through the slots. The cavity is introduced as a four-way power divider to avoid excessive slot spacing. Fig. 1c shows the electric field distributions inside the radiation cavity, from which we can see that the orthogonal slots are excited separately to achieve V-pol and H-pol. It can also be seen that the cavity generates quasi-TE_{420} mode under port 1 excitation and quasi-TE_{240} mode under port 2 excitation. Therefore, highly efficient radiation of V-pol and H-pol is obtained. The two sides of the cross slot are designed to be 12.3 mm and 10.9 mm, respectively, to achieve dual band.

The stacked GWGs and cross-slots are used to achieve orthogonal feeding. Additional metal blocks are added to the input ports to optimize impedance matching by increasing the block thickness. The detailed dimensions of the subarray are listed in Table 1. Fig. 2a describes the simulation results of S-parameters, gain, and radiation patterns. The −10 dB impedance bandwidths of V-pol and H-pol are 13.51–15.01 GHz and 12.15–12.89 GHz respectively, and the isolation is >30 dB. The maximum in-band gains of V-pol and H-pol are 15.30 dBi and

15.03 dBi, respectively. The radiation patterns are given in Fig. 2b. The sidelobes of 14.25 GHz and 12.50 GHz are −12.0 dB and −12.6 dB, respectively.

Table 1 Parameters of the subarray (unit: mm)

Parameter	m_1	l_1	l_2	m_2	m_3	m_4	m_5
Value	13.55	2.3	4.2	12.5	14.05	10.9	12.3

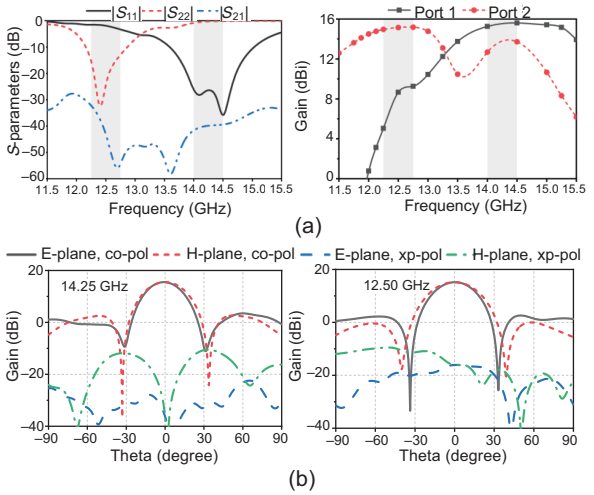

Fig. 2 Simulation results of the unit: (a) *S*-parameters and gain; (b) radiation patterns

The slot spacing is 18.75 mm, about 0.89λ at 14.25 GHz. To avoid sidelobes and grating lobes at a higher frequency, Waffle grids (Ferrando-Rocher et al., 2018) are introduced on the surface of slots to improve the effective aperture area. Fig. 3 demonstrates that the grid narrows the antenna's main beam and increases gain significantly. Fig. 4 further shows the performance of the antenna unit when grid height h_g increases. It represents that the energy distribution within the grids becomes more concentrated with the increase of h_g; thus, the unit gain increases accordingly. The sidelobe also decreases with the increase of h_g when it is smaller than 4 mm, and then rises slightly. To maintain good sidelobe performance, h_g=4 mm is selected to keep a low profile and 3D printing feasibility. The gain of the antenna with 4 mm grids increases by 2.7 dB and the sidelobe decreases by 2.4 dB compared with that without grids.

3 Feeding networks

To achieve compact feeding networks, the power dividers are implemented by RGW. Fig. 5 shows the geometries of all GWG transmission lines used in the

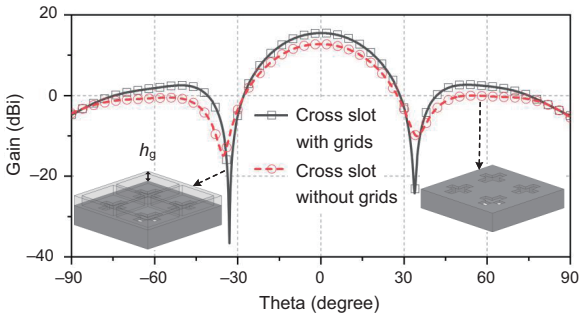

Fig. 3 Radiation patterns with or without grids

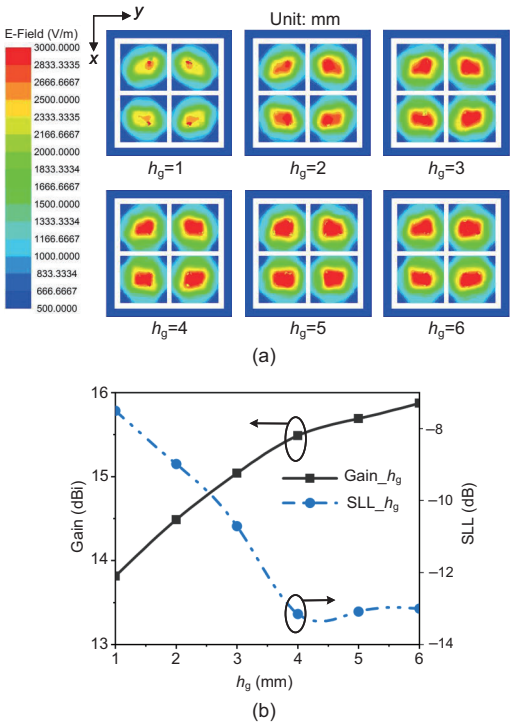

Fig. 4 Performance under different h_g's: (a) electric filed within grids; (b) gain and SLL

feeding networks and the corresponding dispersion diagrams. All of them operate from 10.5 GHz to 18 GHz, perfectly covering the required frequency band. For each polarization, a tapering feeding network composed of bisection and unequal T-junction power dividers is designed to achieve low SLL.

3.1 Unequal T-junction power divider design

This paper presents a new type of unequal T-junction power divider, which has design flexibility and can maintain good phase performance at a high amplitude difference ratio. Fig. 6a shows the geometry of the proposed structure, which introduces a biased rectangular cut angle in the conventional power divider and adds a compensating rectangular block on the other side to maximize the power offset.

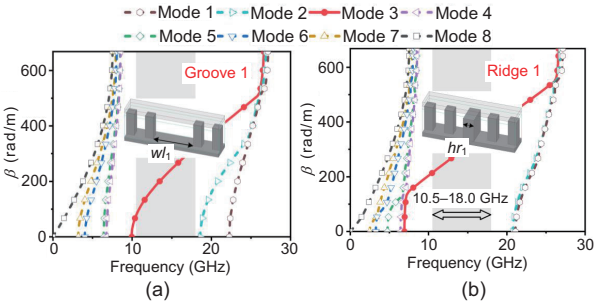

Fig. 5 Geometries and dispersion diagrams of the transmission lines: (a) gap waveguide (GWG); (b) ridge gap waveguide (RGW)

To verify the design flexibility of the proposed structure, its parameters are studied. Since there is structural symmetry between the excision rectangle and the increment rectangle, only v_a, v_b, and v_f are discussed. Figs. 6b–6d depict the simulation results under different parameters. The increase of v_a results in the decrease of the phase difference dramatically and the increase of the amplitude difference slightly. In addition, for any v_a value, the phase difference varies by $\leq 5°$ over the broadband. Increasing v_b can increase the amplitude difference without affecting the phase, and can make the amplitude difference >4.3 dB. Moreover, impedance matching can be optimized by increasing the v_f value. The above discussion proves that the amplitude difference, phase difference, and impedance matching of the proposed structure can be adjusted to the ideal value by relatively independent parameters.

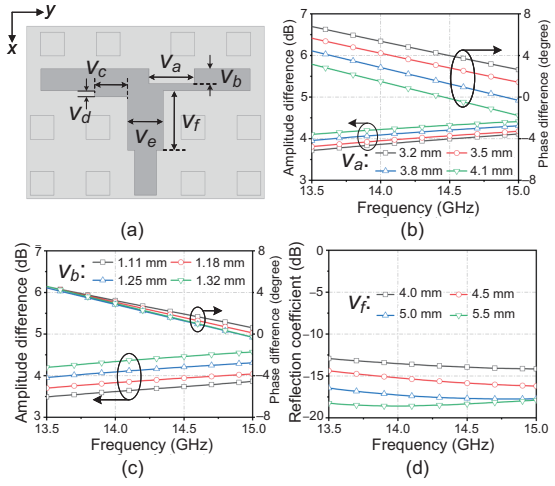

Fig. 6 Geometry and simulation results of the unequal T-junction power divider: (a) geometry; (b) amplitude and phase difference under four different v_a's; (c) amplitude and phase difference under four different v_b's; (d) reflection coefficient under four different v_f's

3.2 Combining feeding networks

The feeding networks for each polarization are depicted in Fig. 7. The power divider is designed by RGW, and two three-step transitions from ridge to groove are designed. For the convenience of testing, the feeding networks are fed by the standard waveguide WR62, so the transitions from waveguide to ridge are designed. Due to the application of transverse slot excitation in the V-pol of the subarray, to avoid the phase reversal of adjacent subarrays, the T-junction power divider in the x-axis direction of feeding network 1 is added with a $\lambda/4$ bending line to compensate for the 180° phase.

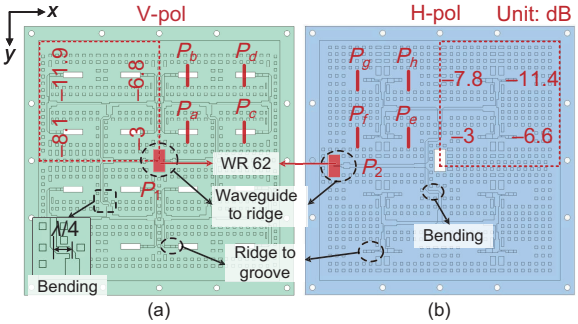

Fig. 7 Geometries of feeding network 1 (a) and feeding network 2 (b)

Taylor amplitude distribution with the desired SLL of –20 dB is used as the initial design. The calculated current weights of each subarray are 0.64:1:1:0.64. The optimized amplitude distributions of the 1/4 network are described in Fig. 7, and unequal power dividers in the x- and y-axis directions are designed according to the amplitude distributions. Fig. 8 plots the simulation results of the feeding networks. The reflection coefficients are less than −15 dB in the required bands. The transmission coefficients of different ports are different, corresponding to the amplitude distribution in Fig. 7.

4 Fabrication and experiment results

Metal 3D printing technology, direct metal laser sintering (DMLS), is used to fabricate the antenna in layers. The metal material is $AlSi_{10}Mg$, with a typical print accuracy of 0.1 mm, and the surface roughness is about R_a=8 μm. The antenna is divided into

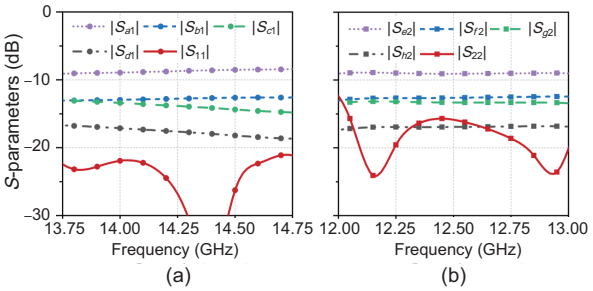

Fig. 8 Simulation results of feeding network 1 (a) and feeding network 2 (b)

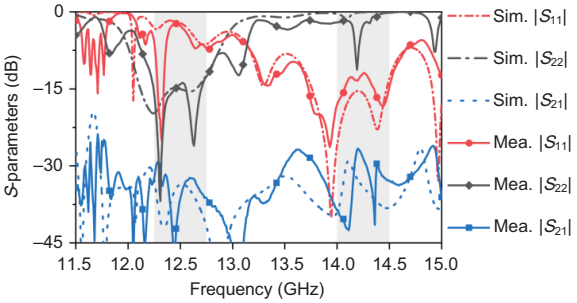

Fig. 10 Measured and simulated *S*-parameters of the antenna

four layers and printed separately. Metal walls are added around the feeding networks to serve as supporting structures and meet the gap height between layers, and round holes are used to assemble the antenna with screws. The top view of the different layers of the fabricated antenna and the measurement setup in the chamber are shown in Fig. 9. The reflection coefficient of the antenna is measured by Keysight N5247B. The gain and radiation pattern of the antenna are obtained by testing in the planar near-field anechoic chamber.

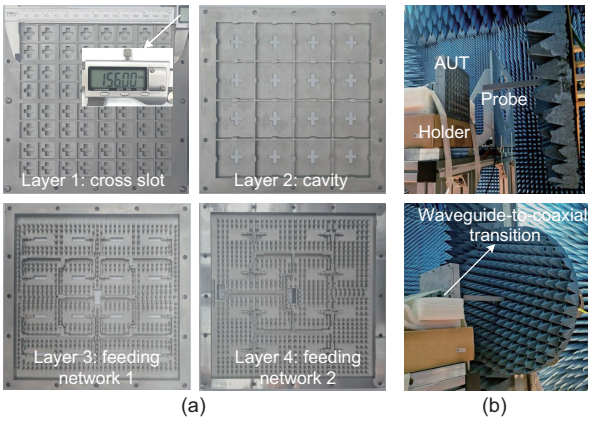

Fig. 9 Different layers of the fabricated antenna and measurement setup: (a) top view of different layers of the antenna; (b) measurement setup in the chamber

Fig. 10 shows the S-parameters of measurement and simulation, from which we can see that the tested impedance bandwidth covers the required frequency bands. The measured and simulated $|S_{11}|$ are in good agreement, while the results of $|S_{22}|$ and $|S_{21}|$ are inconsistent. This is because of the curling produced during the processing of feeding network 2, resulting in an increase in the height of the gap. The measured bandwidths are 6.81% (from 13.62 GHz to 14.58 GHz) for the V-pol port, and 5.12% (from 12.18 GHz to 12.82 GHz) for the H-pol port. The measured isolation is >27 dB.

The measured E- and H-plane far-field normalized radiation patterns of different frequencies under different port excitations are drawn together with the simulation results in Figs. 11 and 12. It can be seen that within the range of ±60°, the test results are in good agreement with the simulation results. The measured SLLs of V-pol and H-pol are lower than −17.4 dB and −18.2 dB, respectively.

The measured gain and radiation efficiency are plotted in Fig. 13. It can be seen that the measured and simulated gain curves tend to be stable and agree well in the band. The maximum measured gains of V-pol and H-pol are both 25.6 dBi with in-band fluctuations of 0.6 dB and 0.4 dB, respectively. The measured radiation efficiency is >72%, which verifies the high efficiency of the antenna.

Table 2 shows a comparison of the proposed slot antenna array with antennas given in the literature. It should be pointed out that, except for the antenna proposed by Yang et al. (2021), the other antennas are based on metal structures, and therefore they have higher gains. In Sun et al. (2022) and Lu et al. (2023), GW-based dual-polarized antennas have good bandwidth and gain levels but are limited to large unit spacing and SLLs higher than −13 dB. The dual-polarized GWG antenna described in Ferrando-Rocher et al. (2019b) not only has higher gain performance and isolation performance, but also has unsatisfactory SLL. Antennas proposed by Huang et al. (2015) and Liu et al. (2022) suppress the sidelobe to a level below −20 dB, but their gain level is lower or comparable, and they can operate only under single polarization. The antenna described by Ran et al. (2022) has a similar SLL to the proposed antenna (both can work with dual polarization), but its gain and radiation efficiency are much lower than

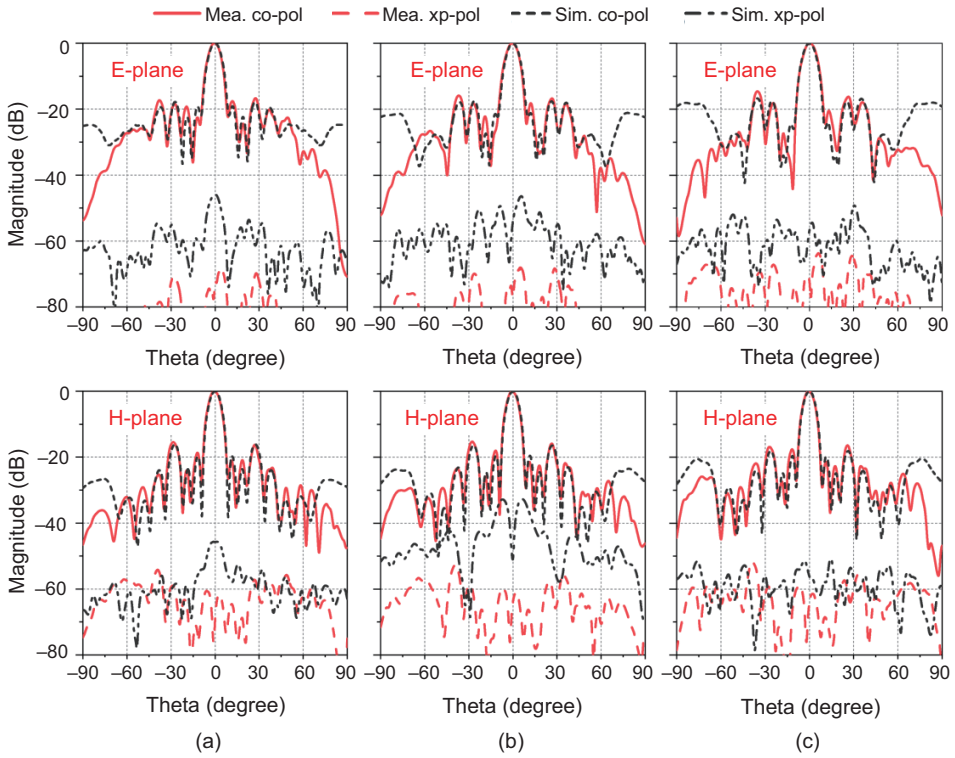

Fig. 11 Measured and simulated normalized far-field radiation patterns of the antenna under V-pol port excitation: (a) 14.00 GHz; (b) 14.25 GHz; (c) 14.50 GHz

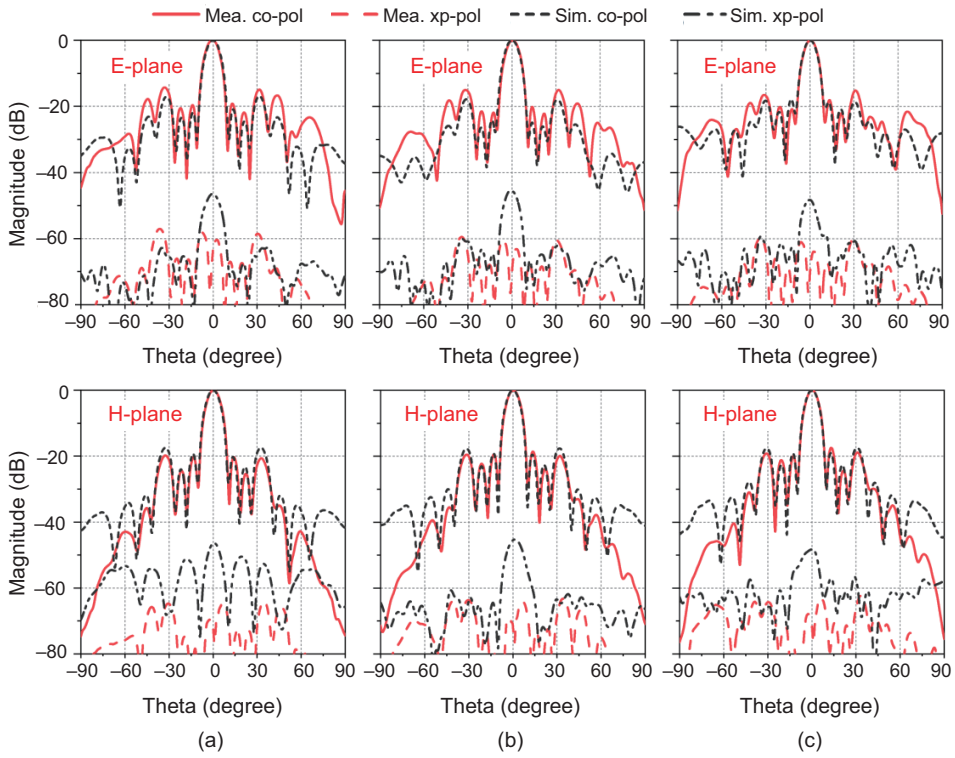

Fig. 12 Measured and simulated normalized far-field radiation patterns of the antenna under H-pol port excitation: (a) 12.25 GHz; (b) 12.50 GHz; (c) 12.75 GHz

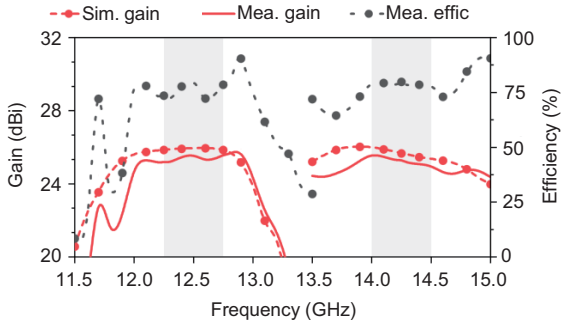

Fig. 13 Measured and simulated gain and efficiency

the counterparts of the proposed antenna. Therefore, it can be concluded that compared with the antennas in the literature, the proposed antenna has both high gain and low SLL.

5 Conclusions

This paper proposes a method for an 8×8 dual-band dual-polarized slot antenna array for Ku-band SATCOM. The radiation element is designed using cavity mode analysis to ensure good gain performance. To eliminate the high SLL caused by excessive slot spacing, the tapered feed distribution is designed, achieving an SLL below −17.4 dB. The antenna array is fabricated by the metal 3D printing process. The measurement results are in good agreement with the simulation results, and the measured efficiency is >72%, which verifies the practicability of the antenna design scheme.

Contributors

Yuqi XIA, Genqiang KOU, and Zihang QI designed the research. Yuqi XIA and Xiuping LI drafted the paper. Wenyu ZHAO, Jie ZHANG, and Muhammad ISHFAQ helped organize the paper. Zihang QI revised and finalized the paper.

Conflict of interest

All the authors declare that they have no conflict of interest.

Data availability

The data that support the findings of this study are

Table 2 Comparison with antenna arrays proposed in the literature

Reference	Feeding network	Polarization	Sidelobe suppression	Number of elements/ Size (λ_0^3)
Yang et al. (2021)	SIW (PCB)	Dual LP	No	8×8/*×*×0.27
Sun et al. (2022)	RW (3D printing)	Dual LP	No	8×8/7.3×7.3×2.6
Lu et al. (2023)	RW (milling)	Dual LP	No	4×4/3.83×3.83×1.88
Ferrando-Rocher et al. (2019b)	GWG (milling)	Dual LP	No	8×8/*×*×*
Huang et al. (2015)	RW (milling)	LP	Yes	16×16/12×12×0.72
Liu et al. (2022)	RW (milling)	LP	Yes	8×8/8.4×8.4×*
Ran et al. (2022)	GWG (milling)	Dual LP	Yes	16×16/*×*×*
This paper	GWG (3D printing)	Dual LP	Yes	8×8/8.47×8.47×1.46

Reference	Impedance bandwidth	Maximum gain (dBi)	SLL (dB)	Efficiency (%)	Isolation (dB)
Yang et al. (2021)	7.5% (19.2–20.7 GHz)	22.8	–14	51	20
Sun et al. (2022)	26.3% (29.1–37.9 GHz) 30.2% (28.7–38.9 GHz)	27.8 28.3	–8	90	36
Lu et al. (2023)	32% (10.5–14.5 GHz)	20.8 21.2	–11.9	79	21.7
Ferrando-Rocher et al. (2019b)	4.6% (29.8–31.2 GHz)	27.3 27.1	–11	75	50
Huang et al. (2015)	13.8% (14.15–16.25 GHz)	30.4	–25	70	–
Liu et al. (2022)	19.2% (71–86 GHz)	25.6	–21	70	–
Ran et al. (2022)	5% (27.26–28.68 GHz) 5.2% (27.5–28.35 GHz)	29.5	–18.5	40	40
This paper	6.81% (13.62–14.58 GHz) 5.12% (12.18–12.82 GHz)	25.6	–17.4	72	27

* Not mentioned. GWG: gap waveguide; SIW: substrate integrated waveguide; LP: linear polarization; RW: rectangular waveguide

available from the corresponding author upon reasonable request.

References

Akbari M, Farahbakhsh A, Sebak AR, 2019. Ridge gap waveguide multilevel sequential feeding network for high-gain circularly polarized array antenna. *IEEE Trans Antenn Propag*, 67(1):251-259. https://doi.org/10.1109/TAP.2018.2878281

Chen M, Fang XC, Wang W, et al., 2020. Dual-band dual-polarized waveguide slot antenna for SAR applications. *IEEE Antenn Wirel Propag Lett*, 19(10):1719-1723. https://doi.org/10.1109/LAWP.2020.3014878

Cheng YJ, Tan FY, Zhou MM, et al., 2020. Dual-polarized wideband plate array antenna with high polarization isolation and low cross polarization for D-band high-capacity wireless application. *IEEE Antenn Wirel Propag Lett*, 19(12):2023-2027. https://doi.org/10.1109/LAWP.2020.3020385

Dimitrov KC, Lee Y, Min BW, et al., 2020. Circularly polarized T-shaped slot waveguide array antenna for satellite communications. *IEEE Antenn Wirel Propag Lett*, 19(2):317-321. https://doi.org/10.1109/LAWP.2019.2961386

Fenech H, Amos S, Tomatis A, et al., 2015. High throughput satellite systems: an analytical approach. *IEEE Trans Aerosp Electr Syst*, 51(1):192-202. https://doi.org/10.1109/TAES.2014.130450

Ferrando-Rocher M, Herranz-Herruzo JI, Valero-Nogueira A, et al., 2018. Single-layer circularly-polarized Ka-band antenna using gap waveguide technology. *IEEE Trans Antenn Propag*, 66(8):3837-3845. https://doi.org/10.1109/TAP.2018.2835639

Ferrando-Rocher M, Herranz-Herruzo JI, Valero-Nogueira A, et al., 2019a. Full-metal K-Ka dual-band shared-aperture array antenna fed by combined ridge-groove gap waveguide. *IEEE Antenn Wirel Propag Lett*, 18(7):1463-1467. https://doi.org/10.1109/LAWP.2019.2919928

Ferrando-Rocher M, Herranz-Herruzo JI, Valero-Nogueira A, et al., 2019b. 8×8 Ka-band dual-polarized array antenna based on gap waveguide technology. *IEEE Trans Antenn Propag*, 67(7):4579-4588. https://doi.org/10.1109/TAP.2019.2908109

Garcia-Marin E, Sanchez-Olivares P, Masa-Campos JL, et al., 2021. Dual circularly polarized array antenna based on corporate feeding network in square waveguide technology. *IEEE Trans Antenn Propag*, 69(3):1763-1768. https://doi.org/10.1109/TAP.2020.3019355

Huang GL, Zhou SG, Chio TH, et al., 2015. A low profile and low sidelobe wideband slot antenna array feb by an amplitude-tapering waveguide feed-network. *IEEE Trans Antenn Propag*, 63(1):419-423. https://doi.org/10.1109/TAP.2014.2365238

Jiang X, Jia FX, Cao Y, et al., 2019. Ka-band 8×8 low-sidelobe slot antenna array using a 1-to-64 high-efficiency network designed by new printed RGW technology. *IEEE Antenn Wirel Propag Lett*, 18(6):1248-1252. https://doi.org/10.1109/LAWP.2019.2913955

Liu PY, Pedersen GF, Zhang S, 2022. Wideband low-sidelobe slot array antenna with compact tapering feeding network for E-band wireless communications. *IEEE Trans Antenn Propag*, 70(4):2676-2685. https://doi.org/10.1109/TAP.2021.3119030

Lu YL, Shen SH, You Y, et al., 2023. Wideband dual linearly polarized hollow-waveguide septum antenna array for Ku-band satellite communications. *IEEE Trans Antenn Propag*, 71(3):2433-2442. https://doi.org/10.1109/TAP.2022.3233626

Miura Y, Hirokawa J, Ando M, et al., 2011. Double-layer full-corporate-feed hollow-waveguide slot array antenna in the 60-GHz band. *IEEE Trans Antenn Propag*, 59(8):2844-2851. https://doi.org/10.1109/TAP.2011.2158784

Ran JQ, Jin C, Zhang PY, et al., 2022. High-gain and low-loss dual-polarized antenna array with reduced sidelobe level based on gap waveguide at 28 GHz. *IEEE Antenn Wirel Propag Lett*, 21(5):1022-1026. https://doi.org/10.1109/LAWP.2022.3155566

Sun FQ, Li YJ, Wang JH, et al., 2022. A millimeter-wave wideband dual-polarized antenna array with 3-D-printed air-filled differential feeding cavities. *IEEE Trans Antenn Propag*, 70(2):1020-1032. https://doi.org/10.1109/TAP.2021.3111502

Yang QL, Gao S, Luo Q, et al., 2021. A dual-polarized planar antenna array differentially-fed by orthomode transducer. *IEEE Trans Antenn Propag*, 69(5):2637-2647. https://doi.org/10.1109/TAP.2020.3028211

You S, Ahn SC, Kim YS, et al., 2022. Asymmetric iris structures for dual-polarization waveguide slot arrays for E-band wireless backhaul systems. *IEEE Trans Antenn Propag*, 70(4):2633-2644. https://doi.org/10.1109/TAP.2021.3118729

Yu L, Yang X, Zhang K, et al., 2023. Millimeter-wave dual-band dual-polarized shared-aperture antenna for satellite communication applications. IEEE MTT-S Int Wireless Symp, p.1-3. https://doi.org/10.1109/IWS58240.2023.10222598

Zaman AU, Kildal PS, 2014. Wide-band slot antenna arrays with single-layer corporate-feed network in ridge gap waveguide technology. *IEEE Trans Antenn Propag*, 62(6):2992-3001. https://doi.org/10.1109/TAP.2014.2309970

Zhang J, Li XP, Qi ZH, et al., 2022. Dual-band dual-polarization horn antenna array based on orthomode transducers with high isolation for satellite communication. *IEEE Trans Antenn Propag*, 70(10):9247-9259. https://doi.org/10.1109/TAP.2022.3177473

Zhang JJ, Zhao DX, You XH, 2022. Analysis and design of a CMOS LNA with transformer-based integrated notch filter for Ku-band satellite communications. *IEEE Trans Microw Theory Tech*, 70(1):790-800. https://doi.org/10.1109/TMTT.2021.3126858

Zhao X, Tian BN, Yeo SP, et al., 2017. Low-profile broadband dual-polarized integrated patch subarray for X-band synthetic aperture radar payload on small satellite. *IEEE Antenn Wirel Propag Lett*, 16:1735-1738. https://doi.org/10.1109/LAWP.2017.2670550